


Original Research

Incremental Diagnostic Value of the Plasma Kynurenine/Tryptophan Ratio for Deep Infiltrating Endometriosis and Its Correlation With Eutopic Endometrial Matrix Metalloproteinase-9 Expression: A Single-Center Prospective Study

Hubin Xu¹, Haimin Jiang¹, Chenmei Ma^{2,*} ¹Hangzhou Normal University, 31112 Hangzhou, Zhejiang, China²Department of Obstetrics, Yongkang Hospital of Traditional Chinese Medicine, 321300 Yongkang, Zhejiang, China*Correspondence: Cm9498156@163.com (Chenmei Ma)

Academic Editor: Osamu Hiraike

Submitted: 29 October 2025 Revised: 8 December 2025 Accepted: 6 January 2026 Published: 26 May 2026

Abstract

Background: Surgery for deep infiltrating endometriosis (DIE) is complex, and current clinical imaging has limited ability to identify and stratify atypical lesions. The kynurenine/tryptophan ratio (KTR) reflects immunometabolic activation, and matrix metalloproteinase-9 (MMP-9) is associated with tissue invasion. **Methods:** This was a single-center prospective study, with pathology as the gold standard. Three analysis populations were defined. KTR was measured by liquid chromatography-tandem mass spectrometry (LC-MS/MS), and MMP-9 by immunohistochemistry (IHC) derived histochemical score (H-score). Multivariable regression, DeLong comparison, calibration and decision curves, and nested F test were used. **Results:** Compared with controls, KTR differed in the DIE and non-DIE groups, with $\beta_{diff} = 0.28/0.15$ (both $p_{adj} < 0.05$). Each 1 SD increase in natural log transformed KTR (lnKTR) was associated with higher ENZIAN stage ($OR_{perSD} = 1.62, p < 0.001$). After KTR was added to the baseline model, the area under the receiver operating characteristic curve (AUC) increased from 0.79 to 0.83 ($\Delta AUC = 0.04, 95\% CI: 0.02-0.07, p = 0.003$). Net benefit increased across the 10%–30% threshold range, and calibration improved from $\alpha = -0.127, \beta = 0.861$ to $\alpha = -0.039$ and $\beta = 0.946$. Among imaging suspected but atypical subjects, net correct reclassification was +14 for events and +17 for non-events. KTR was independently and positively associated with MMP-9 ($\beta_{std} = 0.29, 95\% CI: 0.15-0.43, p < 0.001$), with $\Delta R^2 = 0.04$ ($F = 11.882, p < 0.001$). **Conclusions:** KTR provides an independent and translatable diagnostic increment on current pathways and is associated with eutopic endometrial MMP-9, supporting coupling between systemic immunometabolism and local remodeling. These findings support its use for preoperative stratification and optimization of surgical planning.

Keywords: deep infiltrating endometriosis; kynurenine/tryptophan ratio; diagnostic gain; MMP-9

1. Introduction

Endometriosis is a common chronic disease in women of reproductive age, and the deep infiltrating subtype represents a high burden phenotype with marked invasiveness, increased complications, and greater surgical complexity [1,2]. Current diagnosis and treatment rely on symptoms, clinical examination, transvaginal ultrasound (TVUS), and magnetic resonance imaging (MRI). However, detection of lesions in complex locations or with atypical features remains unstable, and serum carbohydrate antigen 125 (CA-125) shows limited discriminative ability for phenotype and depth of infiltration [3]. Histologically, matrix metalloproteinase-9 (MMP-9) mediates extracellular matrix degradation and fibrotic remodeling and is considered with a marker of tissue infiltration [4]. In terms of immunometabolism, interferon-related pathways can activate the kynurenine pathway by directing tryptophan through indoleamine 2,3-dioxygenase and tryptophan 2,3-dioxygenase. Kynurenine, together with aryl hydrocarbon receptor (AhR) signaling, is hypothesized to contribute

to tissue invasion [5]. The plasma kynurenine/tryptophan ratio (KTR) provides a systemic measure of this pathway has potential as an easily accessible biomarker [6]. Serologic studies targeting the deep infiltrating subtype mostly adopt cross-sectional designs and report receiver operating characteristic (ROC) curves for single biomarkers. They rarely evaluate the independent incremental value beyond real-world clinical and imaging pathways and generally lack evidence of clinical net benefit demonstrated by reclassification or decision curve analysis. A previous study has inadequately controlled key confounders, such as menstrual cycle, exogenous hormones, inflammation, and renal function, and often provide incomplete pre-analytical and laboratory quality-control (QC) information, limiting their generalizability [7]. Key gaps remain regarding whether, under standardized procedures, kynurenine pathway markers show gradient associations with phenotype and infiltration load, whether they provide calibratable incremental value with net benefit beyond a baseline model composed of symptoms, signs, CA-125, and imaging [8], and whether



systemic markers are independently associated with MMP9 in the eutopic endometrium at the individual level. These key gaps limit effective preoperative stratification and surgical planning [9]. In this single-center prospective study, we aimed to clarify the gradient association of the plasma KTR with the phenotype and infiltration load of deep infiltrating endometriosis (DIE) based on existing clinical and imaging pathways, to evaluate its independent incremental contribution to diagnostic performance, and to explore its relationship with MMP-9 expression in the eutopic endometrium. Using rigorous pre-analytical procedures and laboratory validation, plasma KTR was quantified by liquid chromatography-tandem mass spectrometry (LC-MS/MS). A baseline prediction model including symptoms, signs, CA-125, and imaging indicators was constructed, and discrimination, calibration, reclassification, and decision curve analyses were used to evaluate the diagnostic gain provided by KTR. MMP-9 expression in the eutopic endometrium was quantified by immunohistochemistry (IHC), and multivariable regression together with robustness checks was used to examine the association between the systemic immunometabolic marker to local matrix remodeling. The results showed that KTR provided quantifiable diagnostic information with clinical net benefit on top of the existing pathway and was independently and positively associated with MMP-9 expression in the eutopic endometrium, providing an actionable biological basis for preoperative risk stratification and kynurenine pathway-targeted precision interventions.

2. Materials and Methods

2.1 Study Design and Sample Size Estimation

This study was a single-center, prospective, diagnostic gain evaluation with paired histological correlation. The primary objective was to assess the independent incremental value of the plasma KTR for the diagnosis and preoperative stratification of DIE beyond a baseline pathway comprising symptoms, clinical signs, CA-125, and imaging. The paired analysis of eutopic endometrial MMP-9 expression aimed to provide evidence of biological plausibility for KTR as an auxiliary biomarker, rather than a systematic investigation of pathogenesis.

Participants were consecutively enrolled along the clinical pathway. All testing was completed before surgery and pathological determination, and the study team maintained mutual blinding across all components. Ethical approval was obtained prior to study initiation (Approval No. KT2022062), and all participants provided written informed consent. Participants were enrolled from January 1, 2023 to December 31, 2024, and the data were finalized on March 31, 2025. Sample size was pre-calculated based on two primary objectives. Objective 1 considered the difference in the area under the receiver operating characteristic curve (AUC) for KTR added to the “baseline model” (DeLong method, two-sided $\alpha = 0.05$, effect $\Delta\text{AUC} = 0.04$,

event proportion 0.35, correlation coefficient within the prediction population 0.60, power 0.80), requiring a total of 216 participants. Objective 2 assessed the standardized difference in KTR between DIE and non-DIE (Cohen’s $d = 0.5$, two-sided $\alpha = 0.05$, power 0.90), requiring ≥ 85 participants per group. Considering both objectives and an anticipated 10% rate of loss to follow-up or unusable specimens, the planned total sample size was 270, with consecutive enrollment stratified into three categories, DIE, non-DIE endometriosis, and non-endometriosis controls, targeting an approximately balanced distribution to preserve the power of the primary analyses; no fixed quotas were set.

2.2 Study Population

The study population consisted of women of reproductive age scheduled to undergo laparoscopy or laparotomy. Inclusion criteria: age 18–50 years; planned determination of the presence or absence of endometriosis in the current surgery; completion of symptom quantification, pelvic imaging, and blood sampling before surgery; and consent to obtain eutopic endometrial samples at surgery. Exclusion criteria: fever or active infection within the past four weeks; use of systemic glucocorticoids or immunosuppressants within two weeks before surgery; chronic renal insufficiency [estimated glomerular filtration rate (eGFR) $< 60 \text{ mL} \cdot \text{min}^{-1} \cdot 1.73 \text{ m}^{-2}$]; pregnancy or lactation; history of malignancy; inability to complete follow-up; or inadequate specimen handling.

2.3 Outcome Ascertainment and Disease Grading

This study used surgical exploration combined with histopathological examination as the gold standard. Participants were classified by lesion type into three mutually exclusive study groups: ① DIE group: suspicious lesions were found during surgery in deep structures such as the uterosacral ligaments, rectovaginal septum, vaginal fornix, bladder, and bowel wall; histopathology confirmed the presence of endometrial-like glands and/or stroma, and the lesions involved subperitoneal tissue with an infiltration depth $\geq 5 \text{ mm}$, consistent with the definition of DIE; ② non-DIE endometriosis group: histopathology confirmed the presence of endometriosis, but the lesions were confined to ovarian endometriomas and/or superficial peritoneal lesions, without involvement of the above deep structures or not meeting the DIE criterion of infiltration depth $\geq 5 \text{ mm}$; ③ non-endometriosis control group: reproductive-age women scheduled to undergo laparoscopy or laparotomy for benign non-inflammatory pelvic conditions such as uterine fibroids or simple ovarian cysts. All patients underwent standardized TVUS preoperatively, and, when necessary, pelvic MRI within 90 days before surgery to assess for suspicious signs of endometriosis. Intraoperatively, the lead surgeon systematically explored typical sites of involvement, including the pelvic peritoneum, ovaries, uterosacral ligaments, rectovaginal septum, vaginal fornix, bladder,

and bowel wall. Suspicious lesions, such as ovarian cyst walls and peritoneal pigmented or fibrotic areas, were routinely excised or biopsied for pathology. Only when preoperative imaging did not suggest endometriosis, no typical or suspicious endometriotic lesions were seen intraoperatively, and all suspicious lesions were confirmed by pathology to show no endometriosis at any site, the participants were included in the non-endometriosis control group.

All pathological slides were independently reviewed by two senior pathologists blinded to the KTR results, and any discrepancies were resolved by discussion to reach consensus. The primary outcome was the presence or absence of DIE (binary), which was used for diagnostic modeling and gain analyses. At the same time, based on surgical records and imaging data, trained investigators completed the ENZIAN classification, recording the involvement levels of zones A, B, C, and F (grades 0–3), as well as the total number of involved sites, and calculating the overall score [10], to quantify infiltration burden and disease severity.

2.4 Specimen Collection and Laboratory Testing

2.4.1 Plasma KTR Measurement

Within 14 days before surgery, 5 mL of EDTA-anticoagulated blood was collected from the antecubital vein in the early morning under fasting conditions. Within 1 hour after collection, plasma was separated by centrifugation at 4 °C, 1500 g for 10 minutes, aliquoted into pre-cooled polypropylene tubes, stored at –80 °C, with a maximum of one freeze-thaw cycle. The date of last menstrual period, menstrual cycle phase (early follicular phase prioritized for sampling), exogenous hormone use, interval from blood draw to surgery, hemolysis index, and assay batch were recorded. A methodologically validated assay was used to quantify kynurenine and tryptophan, using stable isotope internal standards to correct for matrix effects and recovery. Calibration curves covered 0.5–20 $\mu\text{mol}\cdot\text{L}^{-1}$ for kynurenine and 20–200 $\mu\text{mol}\cdot\text{L}^{-1}$ for tryptophan, with the lower limit of quantification and linear correlation coefficients pre-specified in the validation report and meeting QC acceptance [11]. Low-, medium-, and high-level QC materials were included in each batch, and both within-batch and between-batch coefficients of variation were maintained at 10%. KTR was calculated as the ratio of kynurenine/tryptophan and natural log transformed (lnKTR) to improve distributional characteristics. Laboratory personnel were blinded to clinical groupings and outcomes throughout the study.

2.4.2 Eutopic Endometrial Sampling and MMP-9 Expression Detection

Eutopic endometrial sampling was performed at the start of surgery to avoid interference from intraoperative energy devices. Tissues were immediately fixed in 10% neutral buffered formalin for 24 hours, routinely dehydrated and embedded, and sectioned at 4 μm . A laboratory-

validated rabbit monoclonal anti-MMP-9 antibody was used with heat-induced antigen retrieval in a pH 9.0 buffer, a polymer detection system with 3,3'-diaminobenzidine (DAB) chromogen, and hematoxylin counterstaining. Each batch included both a negative control and a known positive control. Two pathologists, blinded to KTR and outcomes, independently evaluated staining intensity and the percentage of positive cells in glandular epithelium and stromal areas. They calculated the H-score (range 0–300) for each sample. Slides with a difference of >30 points were jointly reviewed to reach a consensus value. The team assessed inter-rater consistency quarterly using duplicate samples and reported the intraclass correlation (ICC) coefficient (target ≥ 0.80). For samples with suspected uncertain cycle phase, a third pathologist reviewed the endometrial phase to ensure consistency with the blood sampling time window.

2.5 Baseline Clinical and Imaging Information

On the same day as blood sampling, symptom assessment was completed, including 10-point visual analog scale scores for dysmenorrhea, chronic pelvic pain, and dyspareunia [12]. Cyclical bowel or urinary symptoms were recorded as binary variables using a structured questionnaire. A senior physician performed a bimanual pelvic examination and recorded posterior fornix tenderness and palpable nodules. Serum CA-125 was measured using a chemiluminescent immunoassay platform, traceable to national reference materials and subjected to daily QC. The imaging protocol followed a TVUS-first strategy performed by trained sonographers, with pelvic MRI supplemented within 90 days before surgery when necessary. Whether DIE was suggested and the total number of involved sites were recorded in a unified manner. The imaging readers and the surgical team were mutually blinded.

2.6 Variable Definitions, Time-Window Alignment, and Confounding Control

The primary exposure variable was lnKTR. The primary outcome was pathology-confirmed DIE analyzed as a binary variable. Secondary outcomes included the ENZIAN grade and the count of involved sites. Pre-specified confounders included age, body mass index (BMI), smoking status, menstrual cycle phase or exogenous hormone use, high-sensitivity C-reactive protein, creatinine, and estimated glomerular filtration rate. Time-window alignment requirements were as follows: symptom scales and physical examination were completed on the same day as blood sampling; the interval between imaging and surgery did not exceed 90 days; the interval between blood sampling and surgery did not exceed 14 days; and the eutopic endometrial sampling was performed concurrently with surgery. Records exceeding the time windows were not included in the primary analyses.

2.7 Statistical Analysis

2.7.1 Chain A: Between-Group Differences and Gradient Trend of KTR With DIE

The analysis first compared differences in KTR among the three groups. Depending on the data distribution, analysis of variance or generalized linear models were used with inclusion of pre-specified confounders, and adjusted mean differences and 95% confidence intervals (CIs) were reported. An ordinal logistic regression model based on ENZIAN grade was constructed to test the gradient trend of KTR. Stratified analyses were performed to assess the consistency of association direction by menstrual cycle phase and exogenous hormone use. Two sensitivity analyses tested the robustness of the results: excluding those with high-sensitivity C-reactive protein $>10 \text{ mg}\cdot\text{L}^{-1}$ and excluding those with an estimated glomerular filtration rate $<60 \text{ mL}\cdot\text{min}^{-1}\cdot 1.73 \text{ m}^{-2}$ [13]. Effect sizes and p-values were two-sided, with a significance threshold of 0.05 ($p < 0.05$).

2.7.2 Chain B: Evaluation of Independent Diagnostic Gain

A pre-specified baseline prediction model was constructed, including symptom quantification, clinical signs, CA-125, and imaging binary indicator and site count. KTR was then incorporated into this model, the AUCs were compared using the DeLong method with optimism correction by bootstrap, and the optimism-corrected AUC difference was reported. Category-based net reclassification improvement and integrated discrimination improvement were calculated according to clinically relevant risk thresholds (10%, 20%, 30%) [14]. Decision curve analysis was used to evaluate changes in net benefit within the above threshold range. Calibration plots and Brier scores were provided, and calibration improvements after adding KTR were reported. For the imaging-suspicious but atypical subgroup, likelihood ratios and changes in pre- versus post-test probabilities were calculated to display the impact of KTR on clinical classification.

2.7.3 Chain C: Multivariable Correlation Between KTR and MMP-9 Expression in Eutopic Endometrium

With MMP-9 H-score as the dependent variable and KTR as the main independent variable, a multiple linear regression model was built with inclusion of pre-specified confounders. Collinearity and residual distributions were examined, and H-score was log transformed or robust regression was used when necessary. Standardized regression coefficients and 95% CIs were reported. Interaction terms were specified for different menstrual cycle phases and exogenous hormone use to evaluate effect modifications. Measurement consistency was verified by the ICC coefficient between the two raters, and measurement error sensitivity analyses of the model were incorporated.

2.7.4 Internal Validation and Sensitivity Analyses

All discrimination models underwent internal validation with 1000 bootstrap resamples to obtain optimism-corrected AUC, calibration slope, and intercept. Three types of sensitivity analyses were conducted for the primary results: including only those sampled in the early follicular phase; excluding those with elevated high-sensitivity C-reactive protein and with renal insufficiency; and stratification by imaging modality. Consistency of results was judged by the direction of effects and the magnitude of change in effect sizes.

2.7.5 Data Management and QC

An electronic case report form was established, with dual independent data entry along with range and logic checks. After source data verification, outliers were corrected. Samples were tracked throughout with barcodes and three-level QC samples. Duplicate samples were randomly interleaved within assay batches to monitor batch effects. Bidirectional blinding was implemented among the clinical team, laboratory, and pathology, and unblinding was performed only after data lock. When the proportion of missing data was $<5\%$, complete-case analysis was applied; when $>5\%$, multiple imputation was performed for covariates and baseline predictors (10 imputed datasets, chained equations), and the exposure and outcome were not imputed. Statistical analyses were performed using R software (version 4.3 or later; R Foundation for Statistical Computing, Vienna, Austria). The main packages included stable versions for ROC comparison, reclassification, and decision curve analysis. All code and analysis logs were archived for future reference after data lock.

3. Results

3.1 Participant Characteristics and Assay QC

A total of 356 candidate participants were assessed, of whom 272 enrolled. Of these, 257 provided samples suitable for pathological evaluation, including 94 DIE, 87 non-DIE endometriosis, and 76 non-endometriosis controls. The study identified three distinct analytical cohorts (Fig. 1). Analysis population A comprised 252 participants with valid KTR (92/85/75). Analysis population B included 234 cases were used to determine diagnostic gain (85/79/70). Analysis population C included 213 cases for the KTR–MMP-9 correlation (79/71/63) (Fig. 1). Kruskal–Wallis and Pearson χ^2 tests showed no statistically significant differences among the three groups in baseline demographics, cycle/hormones, renal function, and smoking status (all $p > 0.05$). Levels of high-sensitivity C-reactive protein (hsCRP) and CA-125 differed significantly among the three groups (both $p < 0.001$). Similarly, the imaging results for suspected DIE and the total count of suspected involved sites showed significant differences (both $p < 0.001$) (Table 1). Method validation and descriptive

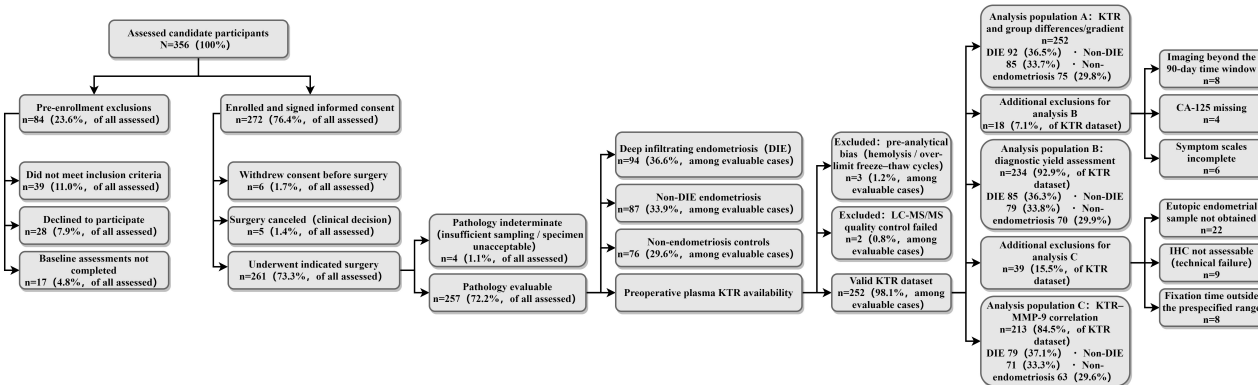


Fig. 1. Flowchart of participant screening, inclusion, and exclusion. DIE, deep infiltrating endometriosis; KTR, kynurenine/tryptophan ratio; IHC, immunohistochemistry; LC-MS/MS, liquid chromatography-tandem mass spectrometry; CA-125, carbohydrate antigen 125.

Table 1. Baseline characteristics of the study population (n, %)/M [IQR].

Variable	DIE group (n = 94)	Non-DIE endometriosis group (n = 87)	Non-endometriosis control group (n = 76)	Statistic	p-value
Demographic and behavioral					
Age (years)	33.7 [28.9–38.6]	32.1 [27.6–37.7]	31.4 [26.5–36.2]	H = 2.713	0.258
BMI (kg·m ⁻²)	22.8 [21.1–25.0]	22.6 [21.0–24.3]	22.7 [21.1–24.6]	H = 0.534	0.766
Smoking status (yes)	13 (13.83%)	10 (11.49%)	9 (11.84%)	χ ² = 0.594	0.743
Smoking status (no)	81 (86.17%)	77 (88.51%)	67 (88.16%)	—	—
Cycle and hormones					
Menstrual cycle phase: follicular phase	52 (55.32%)	46 (52.87%)	40 (52.63%)	χ ² = 0.847	0.932
Menstrual cycle phase: early secretory	24 (25.53%)	22 (25.29%)	18 (23.68%)	—	—
Menstrual cycle phase: late secretory	18 (19.15%)	19 (21.84%)	18 (23.68%)	—	—
Exogenous hormone use (yes)	22 (23.40%)	18 (20.69%)	13 (17.11%)	χ ² = 2.506	0.286
Exogenous hormone use (no)	72 (76.60%)	69 (79.31%)	63 (82.89%)	—	—
Inflammation and renal function					
hsCRP (mg·L ⁻¹)	1.68 [0.92–3.21]	1.22 [0.74–2.15]	0.98 [0.61–1.62]	H = 16.427	<0.001
Creatinine (μmol·L ⁻¹)	67 [60–73]	65 [59–72]	65 [58–71]	H = 1.057	0.589
eGFR (mL·min ⁻¹ ·1.73 m ⁻²)	105 [97–114]	106 [98–114]	107 [99–115]	H = 1.833	0.400
Diagnostic pathway variables					
CA-125 (U·mL ⁻¹)	29.5 [17.6–46.9]	18.7 [12.5–27.9]	13.0 [8.5–18.1]	H = 35.761	<0.001
Imaging modality: TVUS only	51 (54.26%)	46 (52.87%)	49 (64.47%)	χ ² = 6.537	0.162
Imaging modality: MRI only	12 (12.77%)	11 (12.64%)	7 (9.21%)	—	—
Imaging modality: both	31 (32.98%)	30 (34.48%)	20 (26.32%)	—	—
Imaging suggesting DIE (yes)	72 (76.60%)	27 (31.03%)	4 (5.26%)	χ ² = 136.984	<0.001
Imaging suggesting DIE (no)	22 (23.40%)	60 (68.97%)	72 (94.74%)	—	—
Count of suspected involved sites on imaging	2 [1–3]	1 [0–1]	0 [0–0]	H = 91.538	<0.001

M, median; IQR, interquartile range; BMI, body mass index; hsCRP, high-sensitivity C-reactive protein; eGFR, estimated glomerular filtration rate; TVUS, transvaginal ultrasound; MRI, magnetic resonance imaging.

statistics, and an ICC two-way random-effects consistency model were used. The LC-MS/MS calibration range covered 0.50–200.00 μmol/L, with a lower limit of quantification (LLOQ) of 0.50 and 20.00, Bias ranged from –2.27% to

–1.83%, while within-run and between-run CVs remained between 3.29–6.18%. The QC pass rate was ≥97.22% (Table 2A). The IHC scoring demonstrated good to excellent consistency, with overall H-score ICC = 0.892 (95% CI

Table 2A. LC-MS/MS performance.

Parameter	Kynurenine	Tryptophan
Calibration range ($\mu\text{mol/L}$)	0.50–20.00	20.00–200.00
LLOQ ($\mu\text{mol}\cdot\text{L}^{-1}$)	0.5	20
LOD ($\mu\text{mol}\cdot\text{L}^{-1}$)	0.14	6.37
Accuracy (%Bias)	–1.83	–2.27
Within-run CV (%)	3.29	4.06
Between-run CV (%)	4.91	6.18
QC pass rate (%)	98.06	97.22
Hemolysis index range	0–31	0–31
Freeze-thaw cycles (times)	0–1	0–1

LLOQ, lower limit of quantification; LOD, limit of detection; CV, coefficient of variation.

Table 2B. IHC scoring consistency (MMP-9 H-score).

Region	Rater 1 mean H-score	Rater 2 mean H-score	ICC (95% CI)
Glandular epithelium	148.32 \pm 39.14	151.07 \pm 38.22	0.887 (0.851–0.916)
Stromal area	134.26 \pm 35.79	136.11 \pm 34.88	0.874 (0.835–0.906)
Overall H-score	141.59 \pm 36.42	144.05 \pm 35.76	0.892 (0.858–0.920)

MMP-9, matrix metalloproteinase-9; ICC, intraclass correlation.

0.858–0.920), and ICCs of 0.887 and 0.874 for glandular epithelium and stromal areas, respectively (Table 2B).

3.2 Phenotypic Differences and Gradient of KTR With DIE (Chain A)

In Analysis population A, the raw distributions of lnKTR overlapped significantly across the three diagnostic groups, with the median and upper quartile tending to be higher in the DIE group (Fig. 2). Using multivariable linear regression (ANCOVA) and ordinal logistic regression, after adjustment for age, BMI, smoking status, menstrual cycle phase/exogenous hormones, hsCRP and eGFR, the adjusted geometric means of KTR in the DIE and non-DIE endometriosis groups were significantly higher than in the non-endometriosis control group ($\beta_{\text{diff}} = 0.28/0.15$; both $p_{\text{adj}} < 0.05$) (Table 3A). Moreover, each 1 standard deviation (SD) increase in lnKTR was associated with an increase in ENZIAN grade (OR_{perSD} = 1.62, $p < 0.001$) (Table 3B).

3.3 Independent Diagnostic Gain of KTR (Chain B)

Logistic regression modeling was employed for Analysis population B. AUC values were compared using the DeLong method, while the net reclassification improvement (NRI), integrated discrimination improvement (IDI), and their 95% CIs were obtained by 1000 bootstrap resamples. Calibration was assessed with the Brier score accompanied by calibration plots. After adding KTR, AUC increased from 0.79 to 0.83 ($\Delta\text{AUC} = 0.04$, 95% CI: 0.02–0.07, $p = 0.003$). At the pre-specified 20% primary threshold, NRI_{category} = 0.16 ($p = 0.004$), and these results were consistent at the 10% and 30% thresholds. The Brier score decreased from 0.185 to 0.173 ($\Delta = -0.012$), indicat-

ing improvements in discrimination and overall error (Table 4). Decision curve analysis was performed, with 95% CIs obtained by 1000 bootstrap resamples. Within Pt = 0.10–0.30, the “Baseline + KTR” curve lay above “Baseline” across the entire range, showing a sustained and stable magnitude increase in net benefit (Fig. 3A). A logistic calibration model with locally estimated scatterplot smoothing (LOESS) smoothing was used to display predicted–observed agreement. The calibration intercept and slope of the baseline model were $\alpha = -0.127$ and $\beta = 0.861$, indicating slight underestimation; after adding KTR, α approached 0 (–0.039) and β approached 1 (0.946), with calibration markedly improved (Fig. 3B). A risk-band reclassification matrix, a signed-rank test, and the Wilson method were applied (threshold 20%). In the imaging-suspicious but atypical subgroup, after adding KTR the net correct reclassification was +14 for events and +17 for non-events (Table 5A). Pre- versus post-test probability changes showed an increase for events and a decrease for non-events, both $p < 0.001$ (Table 5B). Based on the 20% threshold, the likelihood ratios were positive likelihood ratio (LR+) 3.14 (95% CI 2.07–4.76) and LR– 0.30 (95% CI: 0.17–0.54) (Table 5C).

3.4 Independent Association Between KTR and MMP-9 in Eutopic Endometrium (Chain C)

Analysis population C ($n = 213$) underwent multiple linear regression. MMP-9 H-score was defined as dependent variable, standardized the lnKTR as z-score, log transformed the hsCRP levels, and applied a nested F test to evaluate incremental explained variance. lnKTR was positively associated with MMP-9 in eutopic endometrium ($\beta_{\text{std}} = 0.29$, 95% CI: 0.15–0.43, $p < 0.001$). Among covariates,

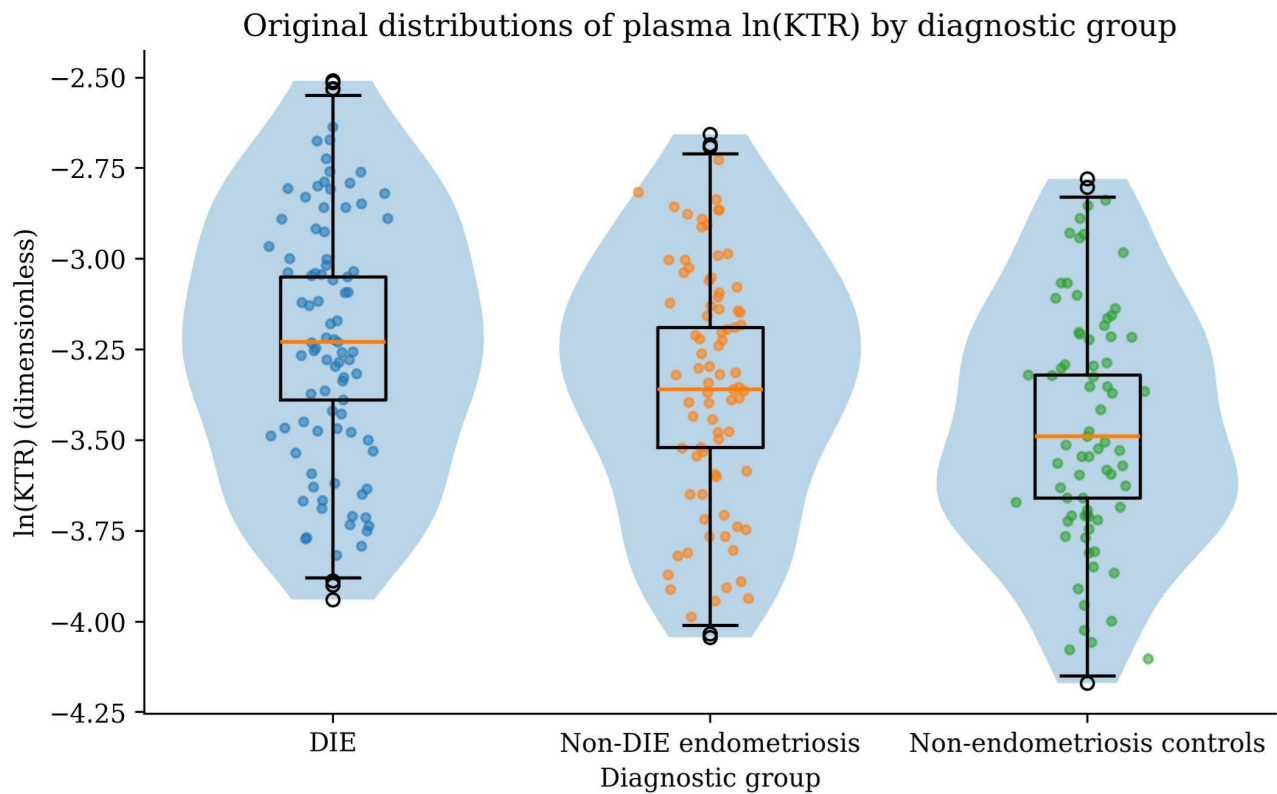


Fig. 2. Raw distribution of plasma KTR across the three diagnostic groups. lnKTR, log transformed KTR.

Table 3A. Adjusted differences in plasma KTR across the three diagnostic groups.

Group	KTR ($\times 10^{-3}$) (95% CI)	β_{diff} (ln ratio) (95% CI)	Wald z	p_{adj}
DIE	40.21 (37.88–42.69)	0.28 (0.16–0.41)	4.39	<0.001
Non-DIE endometriosis	35.22 (33.01–37.59)	0.15 (0.05–0.26)	2.8	0.01
Non-endometriosis controls (reference)	30.31 (28.19–32.52)	—	—	—

Note: Geometric means are back-transformations of model marginal means of lnKTR and are presented as ($\times 10^{-3}$); β_{diff} denotes the difference in log means relative to the non-endometriosis control group.

Table 3B. ENZIAN grade trend analysis.

Predictor	OR_perSD (95% CI)	Wald z	p-value	Brant test χ^2	Brant test p-value
lnKTR (z)	1.62 (1.35–1.94)	4.883	<0.001	4.183	0.523

Note: OR_perSD denotes the odds ratio for a 1 SD increase in lnKTR corresponding to a higher ENZIAN grade.

only ENZIAN total score ($\beta_{\text{std}} = 0.18$), hsCRP (ln) ($\beta_{\text{std}} = 0.13$), and late secretory relative to follicular phase ($\beta_{\text{std}} = 0.11$) were significant (all $p < 0.05$). Model yielded $R^2 = 0.32$, after adding lnKTR, $\Delta R^2 = 0.04$ ($F = 11.882$, $p < 0.001$) (Table 6). The scatter plot, colored by menstrual cycle phase, and the partial regression plot was controlled for all covariates. The overall partial regression line was consistent with the previously described direction, and the point clouds largely overlapped across all phases (Fig. 4).

3.5 Stratified Analyses and Missing Data Sensitivity Analyses

ANCOVA, the DeLong method with NRI_category (20% primary threshold), and multiple linear regression consistent with the main analyses were used. In stratifications of “early follicular only”, excluding hsCRP $> 10 \text{ mg}\cdot\text{L}^{-1}$ /eGFR $< 60 \text{ mL}\cdot\text{min}^{-1}\cdot 1.73 \text{ m}^{-2}$, and by imaging modality (TVUS only versus MRI only), β_{diff} in Chain A, ΔAUC and NRI in Chain B, and β_{std} in Chain C were all positive and significant (all $p < 0.05$). The directions and magnitudes of effects were consistent with the main analyses, indicating robustness (Table 7).

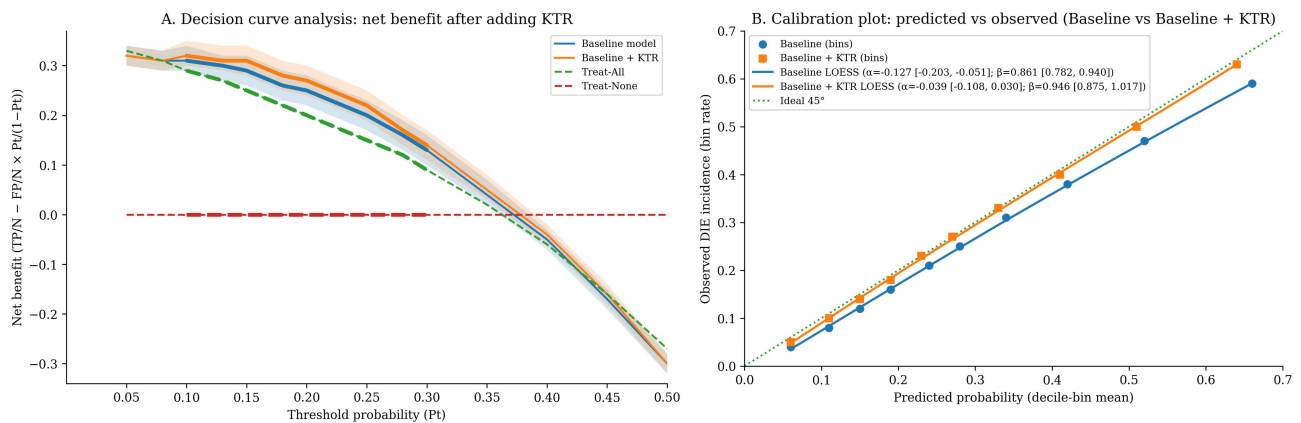


Fig. 3. Clinical benefit and calibration assessment of the models. (A) Decision curve analysis: net benefit after adding KTR. (B) Calibration plot: predicted vs. observed (Baseline vs. Baseline + KTR).

Table 4. Comparison of diagnostic performance between the baseline model and “Baseline + KTR”.

Metric	Baseline (symptoms + signs + CA-125 + imaging)	Baseline + KTR
AUC (95% CI)	0.79 (0.74–0.84)	0.83 (0.79–0.87)
Δ AUC (95% CI)	—	0.04 (0.02–0.07)
p _DeLong	—	0.003
Brier score	0.185	0.173
Δ Brier	—	–0.012
NRI_category (10%/20%/30%, estimate [95% CI])	—	0.18 (0.07–0.29)/0.16 (0.05–0.28)/0.14 (0.03–0.26)
p _NRI (10%/20%/30%)	—	0.001/0.004/0.009
IDI (95% CI)	—	0.04 (0.02–0.07)
p _IDI	—	0.001
AUC (optimism-corrected)	0.78	0.82

Note: Thresholds were defined as 10%, 20%, and 30%; all comparisons were based on the same Analysis population B and covariate set. AUC, area under the receiver operating characteristic curve; NRI, net reclassification improvement; IDI, integrated discrimination improvement.

Table 5A. Risk-band reclassification matrix.

Risk category before adding KTR/Risk category after adding KTR	<10%	10–<20%	20–<30%	\geq 30%	Subtotal (events/non-events)
<10%	1/15	3/5	1/2	0/0	5/22
10–<20%	0/12	3/10	7/6	2/0	12/28
20–<30%	0/2	2/8	6/7	5/2	13/19
\geq 30%	0/2	0/7	2/1	8/2	10/12
Subtotal (events/non-events)	1/31	8/30	16/16	15/4	40/81

Net correct reclassification numbers: events +14 (up-classified 18, down-classified 4); non-events +17 (down-classified 32, up-classified 15). Note: Rows indicate risk categories before adding KTR, columns indicate risk categories after adding KTR, and each cell is presented as events/non-events.

Table 5B. Change in predicted probability before and after adding KTR (Δp = after adding KTR – before adding KTR).

Group	Δp M[IQR]	Z-value	p -value
Events (n = 40)	+0.07 [+0.03, +0.13]	4.086	<0.001
Non-events (n = 81)	–0.05 [–0.10, –0.02]	–4.732	<0.001

Table 5C. Likelihood ratios based on the 20% threshold (after adding KTR).

Metric	Point estimate	95% CI (Wilson)
LR+	3.14	2.07–4.76
LR–	0.30	0.17–0.54

Note: Risk-band thresholds were the same as in Table 4 (<10%, 10–<20%, 20–<30%, ≥30%). Table 5C was based on post-KTR binary classification (threshold 20%): sensitivity = 31/40, specificity = 61/81. LR, likelihood ratio.

Table 6. Multivariable association between KTR and MMP-9 expression in eutopic endometrium.

Independent variable	β _std (95% CI)	SE	t value	p-value
lnKTR (z)	0.29 (0.15–0.43)	0.07	4.143	<0.001
Age	0.06 (–0.04–0.16)	0.05	1.200	0.232
BMI	–0.04 (–0.14–0.06)	0.05	–0.800	0.424
Smoking (yes = 1)	0.05 (–0.07–0.17)	0.06	0.833	0.406
Phase: early secretory (vs. follicular)	0.08 (–0.02–0.18)	0.05	1.600	0.111
Phase: late secretory (vs. follicular)	0.11 (0.01–0.21)	0.05	2.200	0.029
Exogenous hormones (yes = 1)	–0.07 (–0.17–0.03)	0.05	–1.400	0.162
hsCRP (ln)	0.13 (0.03–0.23)	0.05	2.600	0.010
eGFR	–0.03 (–0.13–0.07)	0.05	–0.600	0.547
ENZIAN total score	0.18 (0.06–0.30)	0.06	3.000	0.003

Note: Model R^2 (with KTR): 0.32; ΔR^2 (increment when adding lnKTR to the baseline model without KTR): 0.04; nested model F test (without KTR vs. with KTR): $F = 11.882$, $p < 0.001$.

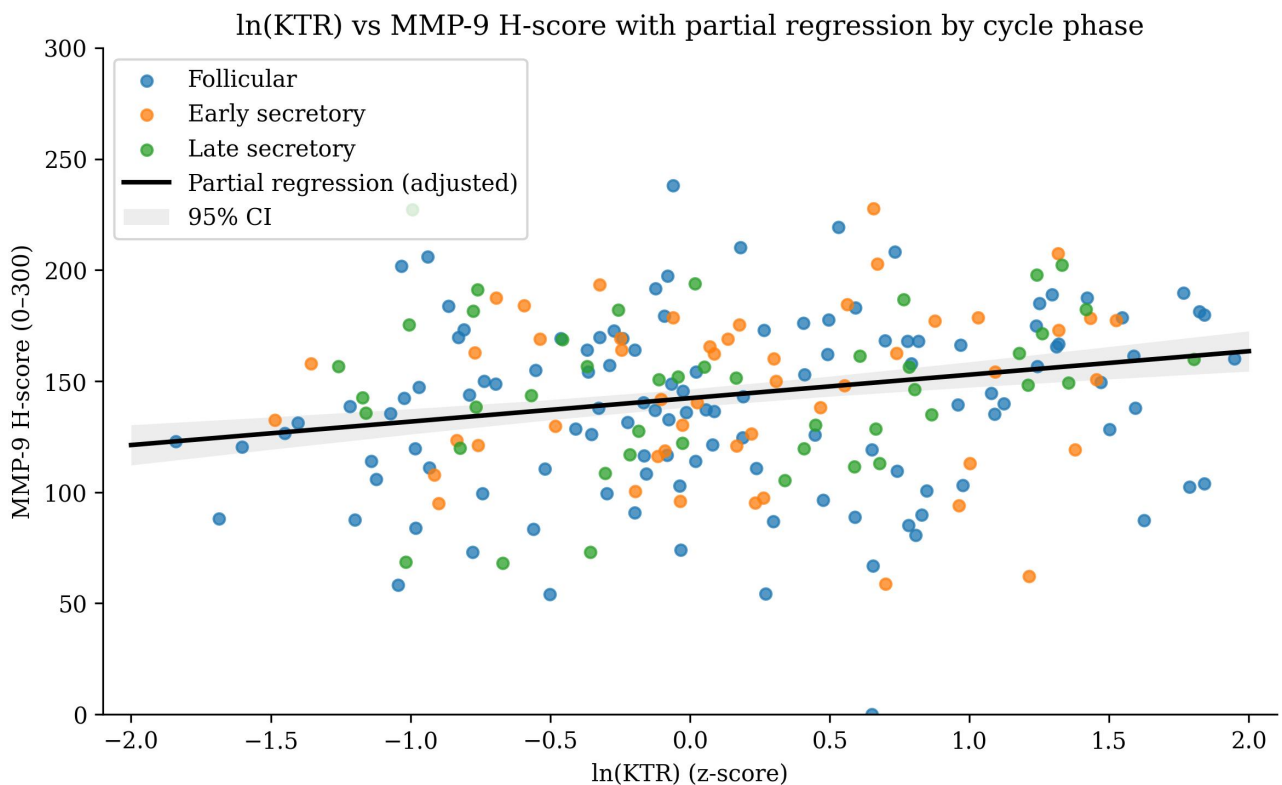


Fig. 4. Scatter plot of KTR (log) versus MMP-9 H-score and partial regression line.

Table 7. Summary of robustness in stratified and sensitivity analyses.

Analysis scenario	Chain A: adjusted β_{diff} of lnKTR for DIE vs. controls (95% CI), p	Chain B: ΔAUC (95% CI), p_{DeLong}	Chain B: NRI_category (95% CI), p	Chain C: β_{std} (lnKTR→MMP-9) (95% CI), p
Early follicular only	0.30 (0.16–0.45), $p = 0.001$	0.05 (0.02–0.08), $p = 0.002$	0.19 (0.07–0.31), $p = 0.002$	0.27 (0.12–0.42), $p = 0.001$
Excluding hsCRP $>10 \text{ mg}\cdot\text{L}^{-1}$ and eGFR $<60 \text{ mL}\cdot\text{min}^{-1}\cdot 1.73 \text{ m}^{-2}$	0.27 (0.14–0.41), $p = 0.001$	0.04 (0.01–0.07), $p = 0.010$	0.17 (0.05–0.28), $p = 0.006$	0.28 (0.14–0.41), $p < 0.001$
By imaging modality: TVUS only	0.26 (0.11–0.40), $p = 0.001$	0.03 (0.003–0.06), $p = 0.047$	0.14 (0.02–0.26), $p = 0.022$	0.27 (0.11–0.41), $p = 0.001$
By imaging modality: MRI only	0.31 (0.16–0.47), $p = 0.001$	0.05 (0.02–0.09), $p = 0.004$	0.21 (0.06–0.35), $p = 0.006$	0.30 (0.13–0.46), $p = 0.001$

Table 8. Variable missingness and imputation settings (Analysis population B, n = 234).

Variable	Missing count (n)	Missing rate (%)	Imputation method (MICE)
Age (years)	2	0.85	PMM
BMI ($\text{kg}\cdot\text{m}^{-2}$)	3	1.28	PMM
Smoking status (yes/no)	5	2.14	Binary logistic
Menstrual cycle phase (follicular/early secretory/late secretory)	8	3.42	Multinomial logistic
Exogenous hormone use (yes/no)	4	1.71	Binary logistic
Dysmenorrhea VAS (0–10)	7	2.99	PMM
Dyspareunia VAS (0–10)	9	3.85	PMM
Posterior fornix tenderness (yes/no)	6	2.56	Binary logistic
hsCRP ($\text{mg}\cdot\text{L}^{-1}$, ln used for modeling)	12	5.13	PMM (on ln values)
eGFR ($\text{mL}\cdot\text{min}^{-1}\cdot 1.73 \text{ m}^{-2}$)	6	2.56	PMM
CA-125 ($\text{U}\cdot\text{mL}^{-1}$)	10	4.27	PMM
Imaging suggesting DIE (binary)	1	0.43	Binary logistic
Count of suspected involved sites on imaging	3	1.28	PMM

Note: Little's MCAR test: $\chi^2 = 18.742$, $p = 0.282$. Because the missing rate of hsCRP was $>5\%$, the diagnostic model used multiple imputation (MICE, $m = 10$, chained equations; including all covariates and imaging indicators, with exposure KTR and outcome DIE not imputed but entered as predictors in the imputation equations).

VAS, visual analog scale; PMM, predictive mean matching.

Table 9. Comparison of sensitivity between complete-case analysis and multiple imputation (Analysis Population B, n = 234).

Metric	Complete cases (CC, n = 206)	Multiple imputation (MI pooled, n = 234; m = 10)
lnKTR (per ↑1 SD) → DIE, OR (95% CI), <i>p</i>	1.57 (1.23–2.04), <i>p</i> = 0.001	1.62 (1.29–2.05), <i>p</i> = 0.001
AUC (Baseline model)	0.79 (0.73–0.84)	0.79 (0.74–0.84)
AUC (Baseline + KTR)	0.83 (0.78–0.87)	0.83 (0.79–0.87)
ΔAUC (DeLong 95% CI), <i>p</i> _DeLong	0.04 (0.01–0.07), <i>p</i> = 0.009	0.04 (0.02–0.07), <i>p</i> = 0.003
Brier score (Baseline → Baseline + KTR)	0.186 → 0.174	0.185 → 0.173
Calibration intercept α (Baseline → Baseline + KTR)	−0.121 → −0.043	−0.127 → −0.039
Calibration slope β (Baseline → Baseline + KTR)	0.865 → 0.944	0.861 → 0.946

CC, complete-case analysis; MI, multiple imputation.

Little’s MCAR test and MICE multiple imputation ($m = 10$) was assessed. Within Analysis population B, the missing data rates for each covariate remained $<5\%$, with the exception of hsCRP, and the missingness pattern was consistent with the MCAR assumption ($\chi^2 = 18.742$, $p = 0.282$) (Table 8). Using logistic regression and the DeLong test, the odds ratio (OR) for DIE per 1 SD increase in lnKTR was similar between complete case and imputed analyses (1.57 vs. 1.62). Moreover, the AUC increased from 0.79 to 0.83, and the directions of improvement in the Brier score and calibration were consistent, indicating that multiple imputation did not alter the main conclusions (Table 9).

4. Discussion

Although the distributions of lnKTR overlapped among the three groups, participants with the deep infiltrating phenotype showed higher median and upper quartile levels when surgical pathology, quantified by ENZIAN, served as the gold standard. After simultaneous adjustment for age, BMI, smoking, menstrual cycle phase, exogenous hormones, hsCRP, and eGFR, this difference remained. The non-DIE endometriosis group also showed higher lnKTR levels than the non-endometriosis controls, and each standard deviation increase in lnKTR corresponded to a higher ENZIAN grade, suggesting a clear dose–response relationship. Stratified and sensitivity analyses showed no reversal of effect direction, and the linearity, precision, and QC pass rate of LC-MS/MS assay, as well as the consistency of IHC scoring, provided technical credibility for the inference. From an immunometabolic perspective, interferon signaling in the inflammatory microenvironment accelerates tryptophan metabolism through indoleamine 2,3-dioxygenase and tryptophan 2,3-dioxygenase pathways, leading to tryptophan depletion and kynurenine accumulation, with KTR rising as a systemic readout of pathway activation [15,16]. As a ligand of AhR, kynurenine can synergize with proinflammatory transcriptional networks, up-regulate MMP expression, and enhance matrix degradation and fibrotic remodeling, conferring stronger adhesion and invasive capacity to lesions [17]. Accordingly, systemic elevation of KTR is consistent with the gradient of deeper tissue infiltration and broader involvement. Previous reports have mostly observed abnormalities of the tryptophan path-

way in mixed endometriosis populations [18], but evidence for discrimination of the deep infiltrating subtype and for quantification of anatomical burden has been insufficient, and control of menstrual cycle and hormonal exposure has often been inadequate. In contrast, the present prospective data, obtained under rigorous preanalytical procedures and multivariable adjustment, demonstrate both phenotypic differences and grading trends, indicating that KTR relates not only to the presence of disease but also to the intensity of the pathological phenotype, providing a testable framework for perioperative stratification and for subsequent mechanistic studies targeting immunometabolism.

After adding KTR to the baseline model composed of symptoms, signs, CA-125, and imaging, discrimination improved, prediction error decreased, probability calibration approached the ideal, and sustained net benefit appeared within the clinically relevant risk range of 0.10–0.30; $\Delta\text{AUC} = 0.04$. Although this represents a numerically moderate increment that commonly appears with a strong baseline model, under the premise that symptoms, signs, and imaging information already integrate into the model, this level of improvement usually corresponds to more substantive risk re-ranking among intermediate-risk patients, especially in preoperative stratification scenarios around the 10%–30% decision thresholds. In the imaging-suspicious but atypical population, addition of KTR achieved net correct reclassification for both events and non-events, shifted individual post-test probabilities in the appropriate direction, and improved likelihood ratios at the 20% threshold. These findings suggest reductions in unnecessary interventions and missed diagnoses in preoperative stratification and management pathways. All these improvements remained robust after internal bootstrap correction. The immunometabolic dimension represented by KTR provides a biological basis for the above phenomena. The conversion of tryptophan to kynurenine through indoleamine 2,3-dioxygenase and tryptophan 2,3-dioxygenase pathways is regulated by inflammatory signals, and an elevated KTR reflects systemic pathway activation [19]. Its information content does not overlap with the structural features captured by imaging or the humoral characteristics of CA-125. When incorporated into the model, it can correct risk ranking and probability calibra-

tion, allowing individuals at intermediate risk near decision thresholds to be adjusted more accurately upward or downward, thereby translating into net benefit within clinically relevant trade-off ranges [20]. High-quality preanalytical control and laboratory validation provided methodological assurance for this gain. A previous serologic study has largely remained at the level of ROC curves for single indicators, have seldom reported calibration metrics and decision curves concurrently, and have lacked evidence of reclassification and likelihood ratios in imaging-atypical scenarios [21]. The present results, evaluated at prespecified thresholds, show concordant improvements in discrimination, calibration, and decision performance, with clinical interpretability presented by the reclassification matrix and likelihood ratios. These findings fill key gaps in the prior evidence chain, indicating that KTR, as an effective supplement to the traditional pathway, has clear clinical translatability.

With surgical pathology as the reference and after adjustment for age, BMI, smoking, menstrual cycle phase, exogenous hormones, high-sensitivity C-reactive protein, estimated glomerular filtration rate, and lesion burden, lnKTR showed an independent positive association with MMP-9 H-score in eutopic endometrium. Partial regression plots showed a stable slope, with point clouds across cycle strata that largely overlapped and stratified, as well as sensitivity analyses pointing in the same direction, suggesting that this association was not driven by cycle differences or covariates such as inflammation or renal function. At the level of immunometabolism, inflammatory signals induce activation of indoleamine 2,3-dioxygenase and tryptophan 2,3-dioxygenase, increasing the flux of tryptophan toward kynurenine [22]. Kynurenine, as a ligand of AhR, can activate downstream transcriptional networks, enhance MMP-9 transcription and secretion, and promote changes in cell adhesion, extracellular matrix degradation, and stromal remodeling, conferring stronger invasive and fibrotic capacity to lesions [23]. The concordant changes in systemic KTR elevation and local MMP-9 enhancement can be interpreted as a coupling marker between immunometabolic signaling and tissue microenvironmental activity [24], supporting the discriminative value of the plasma biomarker for the infiltrative phenotype and providing a measurable bridging index for perioperative risk stratification and potential targeted research. Previous multi-source disease models have suggested that kynurenine and AhR upregulate MMP-9, but population-level evidence in human eutopic endometrium remains scarce [25]. Paired blood-tissue data, combined with consistent robustness checks, fill this key gap by enabling the systemic marker and histologic processes to be compared and verified within the same subjects.

Limitations

To avoid overstating the conclusions, several limitations should be acknowledged. The single-center prospective cohort may be affected by referral and spectrum bias, lacks external and temporal validation, and the stability of risk thresholds has not yet been prospectively tested. NRI, IDI, and decision curves are sensitive to sample size and threshold selection, and their CIs carry inherent uncertainty. KTR is influenced by concomitant inflammation, diet, and metabolic status. Although adjustments were made for hsCRP and renal function, residual confounding may remain. MMP-9 was semi-quantified by IHC, and despite good ICC, batch effects and reader drift may occur. The maximum 90-day interval from imaging to surgery may lead to disease progression. Future work should conduct multicenter, pre-registered external and temporal validation; establish cross-platform standardization of LC-MS/MS and IHC with reference materials; prospectively confirm thresholds according to clinical use scenarios; evaluate decision impact and cost-effectiveness in imaging-atypical and preoperative stratification pathways; combine plasma markers, symptoms, and structural imaging to develop deployable multimodal models; refine preanalytical standard operating procedures (SOPs) and inter-laboratory consistency; and, within the cohort, track longitudinal changes and modifiability of the kynurenine–AhR–MMP-9 pathway to clarify causal associations with clinical outcomes.

5. Conclusions

This study demonstrates that plasma KTR provides independent and quantifiable diagnostic value beyond symptoms, signs, CA-125, and routine imaging. It improves discrimination, calibration, and clinical net benefit, and is particularly useful for preoperative stratification in imaging-suspicious but atypical cases. KTR shows an independent positive association with MMP-9 expression in eutopic endometrium, suggesting an association between systemic immunometabolic activation and local matrix remodeling with clear biological plausibility. Overall, KTR can serve as a practical auxiliary biomarker for DIE to optimize referral and surgical planning and provides a foundation for kynurenine pathway–related precision interventions and multimodal diagnostic models.

Availability of Data and Materials

The datasets used and analyzed during the current study are available from the corresponding author on reasonable request, subject to institutional data sharing policies and ethical approval.

Author Contributions

HX: Conceived and designed the study, participated in patient enrollment and data collection, performed pre-

liminary data analysis, and drafted the first version of the manuscript. HJ: Assisted in study design, performed statistical analysis and data verification, prepared figures and tables, and contributed to revising and polishing the manuscript. CM: Conceived and supervised the overall study, coordinated patient recruitment and clinical data interpretation, provided critical revision of the manuscript for important intellectual content, and serves as the corresponding author. All authors read and approved the final manuscript. All authors have participated sufficiently in the work and agreed to be accountable for all aspects of the work.

Ethics Approval and Consent to Participate

This study was conducted in accordance with the Declaration of Helsinki. The protocol was reviewed and approved by the Ethics Committee of Zhejiang Provincial People's Hospital, Hangzhou, Zhejiang, China (approval No. KT2022062). Written informed consent was obtained from all participants before enrolment in the study.

Acknowledgment

The authors sincerely thank the clinicians, sonographers, and nursing staff of the Department of Obstetrics, Yongkang Hospital of Traditional Chinese Medicine, for their support in participant recruitment, perioperative management, and imaging examinations. We are also grateful to the pathology and laboratory teams for their assistance with specimen processing, LC-MS/MS assays, and immunohistochemical evaluations, as well as to all women who generously participated in this study.

Funding

This research received no external funding.

Conflicts of Interest

The authors declare no conflicts of interest.

Declaration of AI and AI-Assisted Technologies in the Writing Process

During the preparation of this manuscript, the authors used ChatGPT to assist with language editing (including grammar, wording, and style). The authors carefully reviewed and revised all AI-assisted suggestions and take full responsibility. No AI tools were used for data analysis, data generation, or scientific interpretation.

Supplementary Material

Supplementary material associated with this article can be found, in the online version, at <https://doi.org/10.31083/CEOG47790>.

References

- [1] Allaire C, Bedaiwy MA, Yong PJ. Diagnosis and management of endometriosis. *CMAJ: Canadian Medical Association Journal = Journal De L'Association Medicale Canadienne*. 2023; 195: E363–E371. <https://doi.org/10.1503/cmaj.220637>.
- [2] Grube M, Castan M, Drechsel-Grau A, Praetorius T, Greif K, Staebler A, *et al*. Diagnostics and Surgical Treatment of Deep Endometriosis-Real-World Data from a Large Endometriosis Center. *Journal of Clinical Medicine*. 2024; 13: 6783. <https://doi.org/10.3390/jcm13226783>.
- [3] Becker CM, Bokor A, Heikinheimo O, Horne A, Jansen F, Kiesel L, *et al*. ESHRE guideline: endometriosis. *Human Reproduction Open*. 2022; 2022: hoac009. <https://doi.org/10.1093/hropen/hoac009>.
- [4] Ke J, Ye J, Li M, Zhu Z. The Role of Matrix Metalloproteinases in Endometriosis: A Potential Target. *Biomolecules*. 2021; 11: 1739. <https://doi.org/10.3390/biom11111739>.
- [5] Yang HL, Li, MQ. Indoleamine 2,3-dioxygenase in endometriosis. *Reproductive and Developmental Medicine*. 2019; 3: 110–116. <https://doi.org/10.4103/2096-2924.262391>.
- [6] Gáspár R, Halmi D, Demján V, Berkecz R, Pipicz M, Csont T. Kynurenine Pathway Metabolites as Potential Clinical Biomarkers in Coronary Artery Disease. *Frontiers in Immunology*. 2022; 12: 768560. <https://doi.org/10.3389/fimmu.2021.768560>.
- [7] Gibbons T, Rahmioglu N, Zondervan KT, Becker CM. Crimson clues: advancing endometriosis detection and management with novel blood biomarkers. *Fertility and Sterility*. 2024; 121: 145–163. <https://doi.org/10.1016/j.fertnstert.2023.12.018>.
- [8] Vickers AJ, van Calster B, Steyerberg EW. A simple, step-by-step guide to interpreting decision curve analysis. *Diagnostic and Prognostic Research*. 2019; 3: 18. <https://doi.org/10.1186/s41512-019-0064-7>.
- [9] Brulport A, Bourdon M, Vaiman D, Drouet C, Pocate-Cheriet K, Bouzid K, *et al*. An integrated multi-tissue approach for endometriosis candidate biomarkers: a systematic review. *Reproductive Biology and Endocrinology: RB&E*. 2024; 22: 21. <https://doi.org/10.1186/s12958-023-01181-8>.
- [10] Keckstein J, Saridogan E, Ulrich UA, Sillem M, Oppelt P, Schweppe KW, *et al*. The #Enzian classification: A comprehensive non-invasive and surgical description system for endometriosis. *Acta Obstetrica et Gynecologica Scandinavica*. 2021; 100: 1165–1175. <https://doi.org/10.1111/aogs.14099>.
- [11] International Council for Harmonisation (ICH). M10 Bioanalytical Method Validation and Study Sample Analysis. 2022. Available at: https://database.ich.org/sites/default/files/M10_Guideline_Step4_2022_0524.pdf (Accessed: 2 January 2026).
- [12] Cozzolino M, Coccia ME, Lazzeri G, Basile F, Troiano G. Variables Associated with Endometriosis-related Pain: A Pilot Study using a Visual Analogue Scale. *Revista Brasileira De Ginecologia E Obstetrica: Revista Da Federacao Brasileira Das Sociedades De Ginecologia E Obstetrica*. 2019; 41: 170–175. <https://doi.org/10.1055/s-0039-1679879>.
- [13] Kidney Disease: Improving Global Outcomes (KDIGO) CKD Work Group. KDIGO 2024 Clinical Practice Guideline for the Evaluation and Management of Chronic Kidney Disease. *Kidney International*. 2024; 105: S117–S314. <https://doi.org/10.1016/j.kint.2023.10.018>.
- [14] Wang Z, Cheng Y, Seaberg EC, Becker JT. Quantifying diagnostic accuracy improvement of new biomarkers for competing risk outcomes. *Biostatistics (Oxford, England)*. 2020; 23: kxaa048. <https://doi.org/10.1093/biostatistics/kxaa048>.
- [15] Seo SK, Kwon B. Immune regulation through tryptophan metabolism. *Experimental & Molecular Medicine*. 2023; 55: 1371–1379. <https://doi.org/10.1038/s12276-023-01028-7>.
- [16] Midttun Ø, Ulvik A, Meyer K, Zahed H, Giles GG, Manjer J,

- et al.* A cross-sectional study of inflammatory markers as determinants of circulating kynurenines in the Lung Cancer Cohort Consortium. *Scientific Reports*. 2023; 13: 1011. <https://doi.org/10.1038/s41598-023-28135-9>.
- [17] Griffith BD, Frankel TL. The Aryl Hydrocarbon Receptor: Impact on the Tumor Immune Microenvironment and Modulation as a Potential Therapy. *Cancers*. 2024; 16: 472. <https://doi.org/10.3390/cancers16030472>.
- [18] Murgia F, Angioni S, D'Alterio MN, Pirarba S, Noto A, Santoru ML, *et al.* Metabolic Profile of Patients with Severe Endometriosis: a Prospective Experimental Study. *Reproductive Sciences (Thousand Oaks, Calif.)*. 2021; 28: 728–735. <https://doi.org/10.1007/s43032-020-00370-9>.
- [19] Sorgdrager FJH, Naudé PJW, Kema IP, Nollen EA, Deyn PPD. Tryptophan Metabolism in Inflammaging: From Biomarker to Therapeutic Target. *Frontiers in Immunology*. 2019; 10: 2565. <https://doi.org/10.3389/fimmu.2019.02565>.
- [20] Piovani D, Sokou R, Tsantes AG, Vitello AS, Bonovas S. Optimizing Clinical Decision Making with Decision Curve Analysis: Insights for Clinical Investigators. *Healthcare (Basel, Switzerland)*. 2023; 11: 2244. <https://doi.org/10.3390/healthcare11162244>.
- [21] Dolińska W, Draper H, Othman L, Thompson C, Girvan S, Cunningham K, *et al.* Accuracy and Utility of Blood and Urine Biomarkers for the Noninvasive Diagnosis of Endometriosis: A Systematic Literature Review and Meta-analysis. *F&S Reviews*. 2023; 4: 116–130. <https://doi.org/10.1016/j.xfmr.2022.12.001>.
- [22] Zhou Q, Shi Y, Chen C, Wu F, Chen Z. A narrative review of the roles of indoleamine 2,3-dioxygenase and tryptophan-2,3-dioxygenase in liver diseases. *Annals of Translational Medicine*. 2021; 9: 174. <https://doi.org/10.21037/atm-20-3594>.
- [23] Wang Z, Zhang Y, Liao Z, Huang M, Shui X. The potential of aryl hydrocarbon receptor as receptors for metabolic changes in tumors. *Frontiers in Oncology*. 2024; 14: 1328606. <https://doi.org/10.3389/fonc.2024.1328606>.
- [24] Wang Y, Jiao L, Qiang C, Chen C, Shen Z, Ding F, *et al.* The role of matrix metalloproteinase 9 in fibrosis diseases and its molecular mechanisms. *Biomedicine & Pharmacotherapy = Biomedecine & Pharmacotherapie*. 2024; 171: 116116. <https://doi.org/10.1016/j.biopha.2023.116116>.
- [25] Huang Q, Song Y, Lei X, Huang H, Nong W. MMP-9 as a clinical marker for endometriosis: a meta-analysis and bioinformatics analysis. *Frontiers in Endocrinology*. 2024; 15: 1475531. <https://doi.org/10.3389/fendo.2024.1475531>.